LBL-32339
UC-413
Preprint

Lawrence Berkeley Laboratory
UNIVERSITY OF CALIFORNIA

Submitted to Nuclear Physics B

Scale Dependence of Nuclear Gluon Structure

K.J. Eskola

May 1992

For Reference

Not to be taken from this room

NUCLEAR SCIENCE DIVISION

LBL-32339
Copy 1
Bldg. 50 Library.

Prepared for the U.S. Department of Energy under Contract Number DE-AC03-76SF00098

DISCLAIMER

This document was prepared as an account of work sponsored by the United States Government. Neither the United States Government nor any agency thereof, nor The Regents of the University of California, nor any of their employees, makes any warranty, express or implied, or assumes any legal liability or responsibility for the accuracy, completeness, or usefulness of any information, apparatus, product, or process disclosed, or represents that its use would not infringe privately owned rights. Reference herein to any specific commercial product, process, or service by its trade name, trademark, manufacturer, or otherwise, does not necessarily constitute or imply its endorsement, recommendation, or favoring by the United States Government or any agency thereof, or The Regents of the University of California. The views and opinions of authors expressed herein do not necessarily state or reflect those of the United States Government or any agency thereof or The Regents of the University of California and shall not be used for advertising or product endorsement purposes.

Lawrence Berkeley Laboratory is an equal opportunity employer.

DISCLAIMER

This document was prepared as an account of work sponsored by the United States Government. While this document is believed to contain correct information, neither the United States Government nor any agency thereof, nor the Regents of the University of California, nor any of their employees, makes any warranty, express or implied, or assumes any legal responsibility for the accuracy, completeness, or usefulness of any information, apparatus, product, or process disclosed, or represents that its use would not infringe privately owned rights. Reference herein to any specific commercial product, process, or service by its trade name, trademark, manufacturer, or otherwise, does not necessarily constitute or imply its endorsement, recommendation, or favoring by the United States Government or any agency thereof, or the Regents of the University of California. The views and opinions of authors expressed herein do not necessarily state or reflect those of the United States Government or any agency thereof or the Regents of the University of California.

LBL-32339

Scale Dependence of Nuclear Gluon Structure*

K. J. Eskola

Nuclear Science Division, Mailstop 70A-3307
Lawrence Berkeley Laboratory
University of California, Berkeley, CA 94720 USA

Abstract

QCD-evolution of the parton distributions in nuclei is studied by using distributions at an initial scale $Q_0 = 2$ GeV which conserve baryon charge and momentum. Two different Ansätze for shadowing of gluons are considered. The main conclusion in both cases is that shadowing of gluons vanishes much more rapidly with increasing scales Q than shadowing of quarks and antiquarks. We also find that antishadowing of gluons for $x \gtrsim 0.1$ is likely to be limited to $\lesssim 20$ %. As an application, we compute the average inclusive one-jet cross sections in pA and AA collisions at $\sqrt{s} = 200$ and 6500 GeV for $A = 196$.

*This work was supported by the Director, Office of Energy Research, Division of Nuclear Physics of the Office of High Energy and Nuclear Physics of the U.S. Department of Energy under Contract No. DE-AC03-76SF00098.

1. Introduction

In pp and $p\bar{p}$ collisions at very high energies, $\sqrt{s} \gtrsim 200$ GeV, semihard QCD-processes producing minijets, i.e. gluons and (anti)quarks with momentum transfer $p_{\rm T} \gtrsim p_0 \sim 2$ GeV, become increasingly important. This is seen e.g. in the rapid rise of the total inelastic cross sections and in particle multiplicities [1-3]. With increasing energy, information on parton number densities at smaller and smaller x's is needed. For instance, to produce two back-to-back gluon-jets with transverse momentum $p_{\rm T} \sim 2$ GeV and rapidity $y = 0$, typically involves partons with $x = x_{\rm Bj} = 2p_{\rm T}/\sqrt{s} = 0.2$, 0.02, $6 \cdot 10^{-4}$ for $\sqrt{s} = 20$, 200, 6500 GeV, respectively.

The growing importance of semihard processes, in the form of copius production of minijets, is also expected to happen in ultrarelativistic heavy ion collisions at $\sqrt{s} \gtrsim 200$ GeV/nucleon [3,4]. Most of the produced 2 GeV minijets are gluons, and these gluons are expected to contribute significantly to the pre-equilibrium transverse energy densities [3,4] at very high energies. Gluonic minijets may also be important for reaching thermal equilibrium as rapidly as possible [5] to increase the chances of forming a quark-gluon-plasma. The initial temperature is crucial for the rates of thermal photons and dileptons [6]. Thus, it is clear that the initial nuclear *gluon* structure $g_A(x, Q^2)$ at small x and scales $Q \sim p_0$ must be well known to estimate energy densities and temperatures in AA collisions.

In $p\bar{p}$ collisions at $\sqrt{s} = 200$ GeV minijets with $p_{\rm T} \lesssim 5$ GeV are very difficult to observe due to large multiplicities [7], and in ultrarelativistic heavy ion collisions the situation will be even worse. However, jets with larger p_T may be observed. For computing of inclusive $p_{\rm T}$-distributions of jets, it is essential to know the parton distributions in nuclei, $f_A(x, Q^2)$, at scales $Q \sim p_{\rm T}$. Also predictions for other observational quanta which are produced in hard processes of nuclear partons, such as direct photons, primary dileptons and bound states of heavy quarks, require information of the parton distributions in nuclei at higher scales than $Q \sim p_0$.

In deeply inelastic lepton-nucleus scattering experiments it has been observed that there are significant nuclear modifications to the distributions of quarks and antiquarks in free nucleons [8-14]. This means that parton distributions in a nucleus A are not simply given by $f_{i/A}(x, Q^2) = Af_{i/N}(x, Q^2)$, where $f_{i/N}(x, Q^2)$ is the probability of finding a parton i with a momentum fraction x of the momentum of the nucleon N. The scale Q is the momentum scale up to which the parton has QCD-evolved. In these experiments the electromagnetic charge content of quarks and antiquarks in a nucleus, described by the structure function $F_2^A(x, Q^2)$, is probed via a virtual photon. The deep inelastic lA cross sections are proportional to $F_2^A(x, Q^2)$, and the ratio F_2^A/AF_2^N provides us direct information on the nuclear modifications to the quark and antiquark

distributions in nuclei. According to the measurements of the ratio $\frac{1}{A}F_2^A/\frac{1}{2}F_2^D$ there is a clear depletion from unity at $x \lesssim 0.1$ (shadowing) [12-14], and at $0.3 \lesssim x \lesssim 0.7$ (EMC-effect)[8-13]. An increase in this ratio occurs at $0.1 \lesssim x \lesssim 0.3$ (antishadowing) and at $0.85 \lesssim x \lesssim 1$ (Fermi motion) [10,13].

Experimentally, it is observed that shadowing in the F_2-ratio does *not* vanish when the scale Q^2 is increased from $1-2$ GeV^2 up to 10 GeV^2 [13,14]. Theoretically, it was shown by Qiu [15] that solving the Q^2-evolution of the parton densities from the modified Altarelli-Parisi equations [16] leads to the same conclusion. Since quarks and antiquarks have this property, it might seem natural to *assume* that also gluons would behave in the same way with increasing Q^2, that is, that even at higher scales, like $Q^2 \sim m_\Upsilon^2 \sim 100$ GeV^2, one might expect to have strongly shadowed gluons. In this paper we show that in fact the Q^2-evolution, i.e. the QCD-evolution of the gluon distributions in nuclei is most likely significantly *different* from that of the quark and antiquark distributions. The main conclusion of this study is that shadowing of gluons vanishes much more rapidly with increasing Q^2 than shadowing of quarks and antiquarks. This should not be neglected when making predictions for the hard processes in high energy hadron-nucleus and nucleus-nucleus collisions which involve gluon distributions at higher scales than $Q = 1-2$ GeV. Examples of these kind of processes are jet and direct photon production, where Q is basically the transverse momentum exchange between the partons involved, J/Ψ and Ψ' and certainly Υ production, where Q is the mass of the produced bound state, as well as heavy quark and Drell-Yan dilepton production at high invariant masses, where Q is represented by the invariant mass of the pair.

In section 2 we describe how we incorporate the NMC and SLAC deep inelastic lepton-nucleus data for $\frac{1}{A}F_2^A/\frac{1}{2}F_2^D$ [14,10], the E772 data for dilepton production [17] in pA vs. pD collisions and the baryon charge conservation sum rule to determine the valence and sea quark distributions in nuclei at an initial scale $Q_0 = 2$ GeV, motivated by the analysis of ref. [18]. The main problem with the gluon distributions is that there is no direct data for the distributions. What we can actually determine, without using or developing any detailed model for the reduction of the gluon densities at Q_0^2, is only the total momentum carried by the gluons. In spite of many attempts [18-21] there does not seem to be any conclusive model from which gluon shadowing could be rigorously predicted. Therefore, we consider two different Ansätze for $g_A(x, Q_0^2)$. For Ansatz 1, we assume that shadowing of gluons and the ratio $\frac{1}{A}F_2^A/\frac{1}{2}F_2^D$ are identical. For Ansatz 2, we assume an extreme gluon shadowing, motivated by recent provocative analysis of J/Ψ and Ψ' production in pA and πA [22].

In section 3 we plug the parton distributions at the initial scale into the modified Altarelli-Parisi equations, derived by Mueller and Qiu [16]. We then solve the equations

numerically, following footsteps of Qiu [15], to obtain the QCD-evolution towards larger scales Q^2. In this section we present the results in form of the ratios of the parton distributions in a nucleus vs. free nucleons. We also show that the mainline of QCD-evolution in the Q^2-range from 4 GeV^2 to 100 GeV^2 is given by the 'traditional' Altarelli-Parisi equations [24]. Finally, in section 4, we give an application of the obtained scale-dependent parton distributions to the one-jet inclusive cross sections in pA and AA collisions at $\sqrt{s}_{pp} = 200$ and 6500 GeV. Other observational consequences of the QCD-evolution of the scale dependence of nuclear gluon structure are discussed in section 5.

2. Parton distributions at an initial scale Q_0^2

When determining parton distributions in heavy nuclei we are faced with a three-variable problem. In a nucleus A at each fixed momentum scale Q^2, nuclear modifications to the parton distributions are functions of x. Then we have to deal with different momentum scales Q^2, in other words, with QCD-evolution towards higher scales. These two variables are present already at the nucleon level, in the nucleus level the third variable is the mass number A: we have to know the behavior of the parton distributions with increasing A also, since our ultimate goal are the parton distributions in heavy nuclei with $A \sim 200$, like gold (196), lead (209) or uranium (238).

Let us begin our analysis from the deep inelastic lepton-nucleus scattering. In one-photon exchange approximation, the differential cross section per nucleon of a deep inelastic charged lepton scattering from an unpolarized target A is given by

$$\frac{1}{A}\frac{d^2\sigma_{1\gamma}}{dxdQ^2} = \frac{4\pi\alpha^2}{Q^4}\frac{1}{x}\frac{1}{A}F_2^A(x,Q^2)\left[1 - y - \frac{xyM}{2E} + \frac{y^2}{2}\frac{1+4M^2x^2/Q^2}{1+R(x,Q^2)}\right] \qquad (1),$$

where the standard deep inelastic variables are $x \equiv x_{\rm Bj} = Q^2/(2M\nu)$, $y = \nu/E$ with E being the incident lepton energy and ν the energy difference between the incident and scattered lepton in the laboratory frame. The squared 4-momentum of the virtual photon is denoted by $q_\gamma^2 = -Q^2$, the free mass of a nucleon in the target A by M and the ratio of the longitudinally and transversally polarized virtual photon absorption cross sections by $R(x,Q^2)$. Now, if it is assumed that the ratio $R(x,Q^2)$ does not depend on the mass number A of the target, the ratio of cross sections (1) for the nucleus A and $D(A=2)$, gives directly the ratio of the structure functions, $\frac{1}{A}F_2^A/\frac{1}{2}F_2^D$. Experimental results for this ratio, as measured by NMC in μA collisions with 200 GeV muons [14]

and by SLAC in eA collisions with 8-24 GeV electrons [10], are shown in figs. 1 for ^{12}C and ^{40}Ca.

In the QCD-improved parton model the electromagnetic structure function of the nucleons in the target A takes the form

$$\frac{1}{A}F_2^A(x,Q^2) = \sum_{i=\text{flavors}} \left[xq_{i/A}(x,Q^2) + x\bar{q}_{i/A}(x,Q^2)\right] \tag{2}$$

where we have neglected the target-mass corrections [23] and the corrections due to $M_A \neq AM$. Here x is the momentum fraction which a massless parton carries of the total momentum of the nucleus in a frame where the nucleus is moving very fast. The quantity $q_{i/A}(x,Q^2)$ is probability of finding a quark of flavor i with a fraction x of the total momentum of a nucleon in target A. In this context the scale Q is the momentum scale up to which the parton has evolved by emitting QCD-quanta. In principle, if the parton distributions can be determined at some initial scale Q_0, the evolution in Q^2 is predicted by perturbative QCD [24,16].

For a nucleus A with Z protons the structure function $F_2^A(x,Q^2)$ can be written as

$$\begin{aligned} F_2^A(x,Q^2) &= ZF_2^{p/A}(x,Q^2) + (A-Z)F_2^{n/A}(x,Q^2) \\ &= A\frac{1}{2}\left[F_2^{p/A}(x,Q^2) + F_2^{n/A}(x,Q^2)\right] + \frac{1}{2}(A-2Z)\left[F_2^{p/A}(x,Q^2) - F_2^{n/A}(x,Q^2)\right], \end{aligned} \tag{3}$$

where $F_2^{p,n/A}$ are the structure functions in protons and neutrons of the nucleus, respectively. We define the valence quark distributions (in free protons as well as in the protons of the nucleus) u_V and d_V by

$$\begin{aligned} u(x,Q^2) &\equiv \left[u(x,Q^2) - \bar{u}(x,Q^2)\right] + \bar{u}(x,Q^2) \equiv u_V(x,Q^2) + \bar{u}(x,Q^2) \\ d(x,Q^2) &\equiv \left[d(x,Q^2) - \bar{d}(x,Q^2)\right] + \bar{d}(x,Q^2) \equiv d_V(x,Q^2) + \bar{d}(x,Q^2). \end{aligned} \tag{4}$$

In addition, we shall assume that the antiquark sea is flavor symmetric, i.e. $\bar{u}(x,Q^2) = \bar{d}(x,Q^2) = \bar{s}(x,Q^2)$, and, that $s(x,Q^2) = \bar{s}(x,Q^2)$ both in free *and* bound nucleons. In fact, it is probable that, in a nucleus, seaquarks and sea-antiquarks may have different interactions with the probing photon, and therefore slightly different distributions at small x [25]. Since the net charge and the net strangeness of sea must vanish, we expect this difference to be small enough so that we can neglect this complication in the present analysis. With these approximations the ratio of the structure functions of a nucleus A and deuterium becomes

$$\begin{aligned} R_{F_2}^A(x,Q^2) &\equiv \frac{\frac{1}{A}F_2^A(x,Q^2)}{\frac{1}{2}F_2^D(x,Q^2)} \\ &= \frac{5V_A(x,Q^2) + 4S_A(x,Q^2)}{5V(x,Q^2) + 4S(x,Q^2)} + 3(1-\frac{2Z}{A})\frac{d_V^A(x,Q^2) - u_V^A(x,Q^2)}{5V(x,Q^2) + 4S(x,Q^2)}, \end{aligned} \tag{5}$$

where the deuterium is considered as twice an average *free* nucleon, $D = p + n$, the valence distributions are defined as

$$V_{(A)}(x, Q^2) = u_V^{(A)}(x, Q^2) + d_V^{(A)}(x, Q^2) \tag{6}$$

and the sea distributions as

$$S_{(A)}(x, Q^2) = 2\left[\bar{u}_{(A)}(x, Q^2) + \bar{d}_{(A)}(x, Q^2) + \bar{s}_{(A)}(x, Q^2)\right]. \tag{7}$$

Neglecting of nuclear effects in deuterium is justified since it has been shown that e.g. shadowing in D is at most a few per cents [26].

Let us next determine the valence and sea distributions in isoscalar targets. At the moment there are several different models which are successful in describing the data for $\frac{1}{A}F_2^A/\frac{1}{2}F_2^D$, separately in different x-regions (shadowing [18-21, 29,30], EMC effect [31]). However, there is no unique model, and since none of the models covers reliably the whole x-range, we do not want to stick to any particular model at this point, but rather try to see what could be inferred directly from the measured data. Therefore, we first parametrize the deep inelastic lepton-nucleus data of NMC [14] and SLAC [10] for the F_2-ratio (see fig. 1) in the somewhat complicated form described in Appendix. As shown in eq. (A1), we expect the shadowing modifications to $R_{F_2}^A$ to behave as $A^{1/3} - 1$, whereas the A-scaling of the EMC-region is determined from the extensive SLAC data which reaches up to Au. We want the distributions at a lowest scale Q_0 which is still perturbative. The distributions at this scale will then serve as an input data for the QCD-scale-evolution (cf. next section). We shall use $Q_0 = 2$ GeV, since this is the lowest scale one can use when applying the parametrized parton distributions of Duke and Owens [32], and it satisfies the requirement of a perturbative scale [1,2,16,33]. Typically, for the measured points at small x the scales are less than 2 GeV, and at $x \gtrsim 0.3$ they are higher than that. However, the scale dependence of the ratio $R_{F_2}^A(x, Q^2)$ is experimentally observed to be very weak [13,14]. Therefore the choice of the initial scale should *not* have an essential effect in what follows for quarks and antiquarks. For brevity, let us define the ratios of valence, sea and gluon distributions of protons in a nucleus vs. free proton by

$$R_V^A(x, Q^2) \equiv \frac{V_A(x, Q^2)}{V(x, Q^2)}, \quad R_S^A(x, Q^2) \equiv \frac{S_A(x, Q^2)}{S(x, Q^2)}, \quad R_G^A(x, Q^2) \equiv \frac{G_A(x, Q^2)}{G(x, Q^2)}. \tag{8}$$

Besides the deep inelastic lepton data and eq. (5), we have the baryon charge conservation sum rule to restrict the valence quark distribution in nuclei, as pointed out in ref. [18]:

$$\int_0^1 dx V_A(x, Q^2) = \int_0^1 dx V(x, Q^2) = 3. \tag{9}$$

From eq. (5) we see, that $R^A_{F_2} \approx R^A_V$ at large x for an isoscalar nucleus. At very small x we have $R^A_{F_2} \approx R^A_S$, since at the limit $x \to 0$ eq. (9) gives $xV_A \to 0$. The baryon charge conservation immediately rules out the naivest guess that R^A_V could be the same as $R^A_{F_2}$ also at the small-x region: about 20% of the total baryon charge would then be missing for ^{40}Ca, if $R^A_V(x) = R^A_{F_2}(x)$ at all x.

To proceed, we need further restrictions for the antiquark distribution. This is provided by the Drell-Yan cross sections at large x_F. In fig. 1 we display the ratio for Drell-Yan lepton pair yield in ^{40}Ca per nucleon versus the yield in deuterium as measured by the E772 pA experiment with 800 GeV protons [17]. This ratio, at relatively large x_F, gives direct information on the ratio of the antiquark content of a nucleus vs. deuterium. This is easy to see by writing down the lowest order result for the ratio of the differential cross sections per nucleon for Drell-Yan pair production in pA versus pD:

$$\left[\frac{1}{A}\frac{d\sigma^{pA}_{\rm DY}}{dx_{\rm F}dM^2}\right]\cdot\left[\frac{1}{2}\frac{d\sigma^{pD}_{\rm DY}}{dx_{\rm F}dM^2}\right]^{-1} =$$
$$\Big\{R^A_S(x_2,M^2)\cdot\big[5V(x_1,M^2)+4S(x_1,M^2)\big]S(x_2,M^2)+R_V(x_2,M^2)\cdot 5S(x_1,M^2)\cdot$$
$$\cdot V(x_2,M^2)\Big\}\cdot\Big\{\big[5V(x_1,M^2)+4S(x_1,M^2)\big]S(x_2,M^2)+5S(x_1,M^2)V(x_2,M^2)\Big\}^{-1}, \tag{10}$$

where $x_{1,2} = \frac{1}{2}(\sqrt{x_{\rm F}^2 + 4M^2/s} \pm x_{\rm F})$, with M the invariant mass of the lepton pair and $\sqrt{s}$ the hadron-hadron CMS energy. In (10) we used the same approximations and definitions as described above and expressed the ratio for an isoscalar target. At large $x_{\rm F}$ ($x_F \gg 2M/\sqrt{s}$) the first term in the nominator clearly dominates, and the ratio (10) gives directly $R^A_S(x_2)$.

Since no clear *anti*shadowing is seen in the E772 data, we assume that $R^A_S \sim 1$ at $0.08 \lesssim x \lesssim 0.3$. Clearly, the data is not conclusive at $x \gtrsim 0.15$, and we don't get experimental information on the sea distributions in this region from the SLAC data since $R^A_{F_2}$ is dominated by valence distributions. Therefore we simply assume that R^A_S coincides with $R^A_{F_2}$ at $x \gtrsim 0.3$. In practice, in all the applications we are interested in, antiquark distributions at large x do not contribute, and have a negligible contribution to the total momentum, too.

Now, we can use our parameterization (A1) of $R^A_{F_2}$ to determine R^A_V and R^A_S: the missing antishadowing in R^A_S results an excess in R^A_V with respect to $R^A_{F_2}$ around $x \sim 0.1$. Then the baryon charge conservation rule (9) forces R_V to be much less shadowed than R^A_S, as seen in fig. 1, which in turn determines R^A_S at small x from eq.

(5). For R_V^A at small x we use the form of the parameterization (A1) with adjusted parameters. At this point we do not agree with ref. [18], where the shadowing of valence quarks is claimed to be stronger than shadowing of seaquarks at very small x. The physical reason for the smaller shadowing of valence quarks is, as far as we can see, simply the smaller number densities at small x. In the recombination explanation of shadowing [20] the corrections to the parton distributions should be proportional to the distributions of recombining partons, and, at small x the valence quark densities are far less than the corresponding seaquark densities. In addition to this, antiquarks reflect also the shadowing of gluons. Furthermore, it should be kept in mind that the division of the quark-distribution into valence and sea (eq. (4)) is somewhat artificial; our result simply implies that quarks are less shadowed in a nucleus than antiquarks, which seems like a natural consequence of the production mechanism of antiquarks from gluons and interactions with them.

We get quite a good harmony between the NMC and SLAC lA data for $R_{F_2}^A$, E772 Drell-Yan pA data for R_S^A, combined to our parameterization of $R_{F_2}^A$, eq. (A1), and to the baryon charge conservation (9), as seen in figs. 1a and b. According to eq. (5) in non-isoscalar targets the correction term due to difference in the numbers of protons and neutrons is small: at very small x it vanishes, and at larger x, for e.g. A=196, the relative contribution is at most a few per cent. We therefore neglect the correction term in eq. (4) and extrapolate from $A = 40$ up to $A \sim 200$ by using the parameterization (A1). Ratios of the parton distributions in a gold nucleus are shown in figs. 2 and 3 (the lines with Q=2 GeV). In theses figures, we have also displayed the ratio R_S^A from the E772 Drell-Yan data in pW and the ratio $R_{F_2}^A$ from the SLAC deep inelastic scattering data in eAu collisions. The extrapolation to heavy nuclei seems to work well for the seaquarks also. To further test applicability of our parameterization, we have checked e.g. that while the baryon charge is conserved for ^{40}Ca, it is still conserved within 3.5% when extrapolating to $A = 196$.

In the following, let us move on to gluons in nuclei. Using the momentum conservation sum rule, again as stressed in ref. [18]:

$$\begin{aligned} 1 &= \int_0^1 dx\left[xV_A(x,Q^2) + xS_A(x,Q^2) + xG(x,Q^2)\right] \\ &= \int_0^1 dx\left[xV(x,Q^2) + xS(x,Q^2) + xG(x,Q^2)\right]. \end{aligned} \tag{11}$$

We can now compute the proportion of the total momentum that is carried by gluons at the initial scale $Q_0 = 2$ GeV. We find that gluons carry 2-3% more momentum in ^{40}Ca (about 4% in ^{196}Au) than they do in a free proton.

If there were no x-structure in the ratio R_G^A at all, there should be a horizontal line at 1.02 at fig. 1b. However, most probably this is not the case, but also gluons exhibit nuclear modifications besides the small amount of momentum flown from quarks and antiquarks into gluons (see also discussion). None of the present models [18-21] is capable to reliably predict the exact amount of shadowing of gluons as a function of x (at Q_0), not to mention the mid-x region behavior of R_G^A. Further complication is that there is no such direct experimental data for the ratio R_G^A as there exists for $R_{F_2}^A$ and R_S^A. Therefore we wish to treat two possible Ansätze for the gluon distributions at the initial scale.

In the **first Ansatz for gluons** we *assume* that gluons are shadowed by about the same amount as the ratio $R_{F_2}^A$. This fulfills the plausible expectation that $R_G^A \gtrsim R_S^A$ at small x [15,20]. Since seaquarks are produced by gluons their shadowing should be of the same order as of gluons. In addition, seaquarks may recombine with gluons and antiquarks, i.e. they have an additional mechanism for suppression, and therefore they should be more shadowed than gluons. The assumption $R_G^A \approx R_{F_2}^A$ at small x is also in agreement with the claims in refs. [18,19], as well. We want to consider the simplest possible case for gluons, i.e. we assume that all the momentum what is missing at small x is evenly distributed into the region of larger x. Strictly speaking this is of course not quite true, since near $x \sim 1$ the ratio R_G^A should shoot up anyway, because of the zero-gluon-density in a free proton. But, again, from our point of view this is not an essential point, since the large-x region does not practically contribute to the momentum conservation, nor to the perturbatively calculable hard processes. Consequently, this simplification is accurate enough an approximation for our purposes, and does not affect the main line of this study. The gluon ratios $R_G^A(x, Q_0^2)$ obtained in this way are shown in figs. 1.

In the **second Ansatz for gluons** we make use of the E772 data on J/Ψ and Ψ' production in pW collisions [34] and the NA3 data on J/Ψ production in πA and pA collisions [35]. As discussed in ref. [22], for $x_{\rm F} \lesssim 0.4$ the cross sections of producing J/Ψ and Ψ' are strongly dominated by the gluon-gluon fusion, and therefore the ratio of the cross sections of e.g. J/Ψ production in pA vs. in pD describe $R_G^A(x_2, M_{\rm J/\Psi}^2)$ with corrections less than 10% in this x-region, *if* all the final state interactions of the produced heavy-quark pair can be neglected. Following ref. [22], we convert the measured ratios of the yields in heavy nuclei vs. deuterium for J/Ψ and Ψ' resonances with $x_F \lesssim 0.4$ into functions of $x_2^{\rm W} = \frac{1}{2}(\sqrt{x_{\rm F}^2 + 4M^2/s} - x_{\rm F})$. The converted datapoints are shown in fig. 3a. It should be noticed, that in this way we get information on the gluon distributions in nuclei only at $Q \sim M_{J/\Psi} \sim 3$ GeV, i.e. *not* at our lower initial scale $Q_0 = 2$ GeV (this point will be clarified in the next section where the scale evolution is discussed). However, since the errorbars of the data for Ψ' are relatively

large, and since final state effects of the resonances were neglected, we let the data only be our guide, and we draw the gluon ratio at small x as shown in fig. 3a by the line with $Q = 2$ GeV. Conservation of momentum, eq. (11), causes the excess again at larger values of x. By claiming that gluons could be this strongly shadowed, we have to give up the expectation that $R_G^A \gtrsim R_S^A$ at small x and at relatively low values of the scale Q^2. The Ansatz 2 is thus an extreme case for gluon shadowing.

3. Scale evolution of the parton distributions in nuclei

Next thing to worry about, after determining the parton distributions in nuclei at an initial scale Q_0^2, is their QCD-evolution towards higher values of Q^2. In the case of free protons, this can be obtained from perturbative QCD, in form of the Altarelli-Parisi (AP)-equations [24]. In nuclei, however, the evolution is not just independent emission of QCD-quanta from A nucleons, but there are several recombination processes to reduce the number of partons in nuclei at small x as discussed in detail in ref. [16]. Mueller and Qiu [16] have calculated the recombination probabilities for gluons to go into gluons or into quarks in the low density limit ($Q \geq Q_0 \sim 2$ GeV), resulting modification terms to the 'usual' AP-equations of seaquarks and gluons. However, also in the case of nuclei, the mainline of QCD-evolution is given by the traditional AP-equations, as will be seen.

For the ratio $R_{F_2}^A$, evolution in Q^2 should be quite slow, which is evident from the data [13,14]; $R_{F_2}^A$ does not alter very much when the scale is increased from $Q^2 = 1$ GeV^2 to $Q^2 = 10$ GeV^2. This was confirmed by Qiu in ref. [15]. On the other hand, we know from the AP-scale-evolution of the parton densities in a free proton that there is a momentum flow from quarks and antiquarks into gluons, as well as a change in the number densities of partons towards smaller x's when Q^2 grows. The same QCD-evolution happens also in nuclei: momentum is flowing into gluons, and the gluon distribution becomes more peaked at low x. Can momentum conservation anymore hold if R_G^A does not change at higher scales? Even if quarks and antiquarks may maintain roughly the same ratios R_V^A and R_S^A with increasing scale it is not at all obvious that this should apply for gluons as well. In the following, we shall see that, indeed, R_G^A behaves *differently* from $R_{F_2}^A$.

The modified AP-equations [16] were first solved numerically by Qiu [15], but at that time there was not as high precision data available as we have today, and realistic determination of the parton distributions at an initial scale was fairly impossible. Since now we believe we have relatively good control over the parton distributions at Q_0,

except for the gluons, it is a meaningful task to solve the (modified) evolution equations numerically again and report the results as ratios $R_G^A(x,Q^2)$, $R_S^A(x,Q^2)$ and $R_V^A(x,Q^2)$ and compare the ratio $R_{F_2}^A$ to the one obtained from the deep inelastic lepton-nucleus data.

In the following, we write down the lowest order QCD-evolution equations in terms of the splitting functions P_{ij} [24] and take the MQ-modification terms from ref. [16]. As done in ref. [15], also we write down the equations separately for flavor nonsinglet part xV_A, flavor singlet sea part xS_A and gluons xG_A:

$$Q^2\frac{\partial}{\partial Q^2}xV_A(x,Q^2) = \frac{\alpha_s(Q^2)}{2\pi}\int_x^1 \frac{dy}{y} zP_{qq}(z)\cdot yV_A(y,Q^2), \tag{12}$$

$$\begin{aligned} Q^2\frac{\partial}{\partial Q^2}xS_A(x,Q^2) = {} & \frac{\alpha_s(Q^2)}{2\pi}\int_x^1 \frac{dy}{y}\left[zP_{qq}(z)\cdot yS_A(y,Q^2) + 2N_f zP_{qg}(z)\cdot yG_A(y,Q^2)\right] \\ & - \frac{\bar{n}_2^A}{Q^2}\left[\mathcal{R}^{(1)}_{gg\to q}(x,Q^2) + \mathcal{R}^{(2)}_{gg\to q}(x,Q^2)\right], \end{aligned} \tag{13}$$

$$\begin{aligned} Q^2\frac{\partial}{\partial Q^2}xG_A(x,Q^2) = {} & \frac{\alpha_s(Q^2)}{2\pi}\int_x^1 \frac{dy}{y}\left[zP_{gq}(z)\cdot\{yV_A(y,Q^2) + yS_A(y,Q^2)\}\right. \\ & \left. + zP_{gg}(z)\cdot yG_A(y,Q^2)\right] - \frac{\bar{n}_2^A}{Q^2}\mathcal{R}_{gg\to g}(x,Q^2), \end{aligned} \tag{14}$$

where $z = x/y$ and $\bar{n}_2^A = \frac{9}{8}\frac{A}{\pi R_A^2}$,

$$\mathcal{R}_{gg\to g}(x,Q^2) = \frac{4\pi^3}{N^2-1}\left(\frac{\alpha_s C_A}{\pi}\right)^2\int_x^1 \frac{dy}{y}\left[yG_A(y,Q^2)\right]^2, \tag{15}$$

$$\mathcal{R}^{(1)}_{gg\to q}(x,Q^2) = \frac{4\alpha_s^2(Q^2)T_f\pi}{N(N^2-1)}\left[\frac{4}{15}N^2 - \frac{3}{5}\right]\left[xG_A(x,Q^2)\right]^2 \tag{16}$$

$$\mathcal{R}^{(2)}_{gg\to q}(x,Q^2) = -\frac{2\alpha_s(Q^2)T_f}{\pi}\int_x^1 \frac{dy}{y} z\bar{\gamma}_{\rm FG}(z) yG_A^{\rm HT}(y,Q^2) \tag{17}$$

where $T_f = \frac{1}{2}$, $C_A = N = 3$, $\bar{\gamma}_{\rm FG}(x) = -2x + 15x^2 - 30x^3 + 18x^4$ and

$$Q^2\frac{\partial}{\partial Q^2}yG_A^{\rm HT}(y,Q^2) = -\mathcal{R}_{gg\to g}(y,Q^2) \tag{18}$$

For the higher dimensional gluon input distribution at the initial scale we have used an ansatz $xG_A^{\rm HT}(x,Q_0^2) = \left[xG_A(x,Q_0^2)\right]^2$ of ref. [15]. As discussed by Qiu, this function is basically uncalculable, but its effect relatively small as compared to the leading AP-terms, and does not have a crucial effect to the final results. We consider only light quarks, so we solve the eqs. (12-14) with $N_f = 3$.

First we solve the full evolution equations above for partons in free protons and partons in protons of a nuclei. In figs. 2 and 3. we show the obtained ratios $R_G^A(x,Q^2)$, $R_V^A(x,Q^2)$ and $R_S^A(x,Q^2)$ as well as $R_{\rm F_2}^A(x,Q^2)$ for $A = 196$ in the two Ansätze we have for gluons. We have plotted the results at $Q = 2, 3, 5, 7$ and 10 GeV. As expected, we confirm the results of Qiu about the very slow vanishing of shadowing for the ratio $R_{\rm F_2}^A$: both in fig. 2c and 3c the difference between the curves with $Q = 2$ GeV and $Q = 3$ GeV is small. The curves for ^{40}Ca are not shown but we have checked that the scale evolution in the ratio $R_{F_2}^{\rm Ca}$ from $Q_0 = 2$ GeV to $Q = 3$ GeV indeed is slow enough to agree with the measured data [14]. We conclude that the scale evolution of $R_{F_2}^A$ falls well inside the errorbars of the NMC-data [14] at respective scales in the experiments ($Q^2 = 0.5 - 10$ GeV^2 at the shadowing region). In addition, from fig. 3 we see that the more shadowed gluons are, the slowlier does the shadowing in the F_2-ratio vanish. The physical reason for this is simply that since there are fewer gluons filling up the small-x region, there are also fewer sea-quarks produced in the same region, so the filling of the seaquark-shadowing region is thereby slower.

To check the effect of the MQ-modifications, we solved eqs. (12-14) also without the $\sim \bar{n}_2^A/Q^2$ terms. The results are shown in figs. 4. We find that, e.g. for $A = 196$ at $Q = 2 - 10$ GeV, the AP-equations alone describe the QCD-evolution with accuracy of 6-7% when the Ansatz 2 for gluons is considered. However, the MQ-modifications drive parton distributions towards slower Q^2-evolution, i.e. towards the trend observed experimentally for $R_{F_2}^A$.

Our picture seems to be consistent also with the E772 Drell-Yan data [17], since the scales in that experiment were somewhat higher ($Q = M \gtrsim 4$) than our initial scale: when Q^2 is increased from 4 GeV^2 to 16 GeV^2, we get even better fit to the shadowing part of the E772 data, as seen in figs 2-3.

Nonvanishing of shadowing in the valence quark distributions at very small x can be understood as follows. We can analytically solve from eq.(12)

$$\begin{aligned}\frac{Q^2}{R_V^A(x,Q^2)}\frac{\partial R_V^A(x,Q^2)}{\partial Q^2} &= \frac{Q^2}{xV_A(x,Q^2)}\frac{\partial xV_A}{\partial Q^2} - \frac{Q^2}{xV(x,Q^2)}\frac{\partial xV}{\partial Q^2} \\ &= \frac{2\alpha_s}{3\pi}\frac{1}{V(x,Q^2)}\int_x^1 dy\frac{1+(x/y)^2}{y-x}\left[\frac{R_V^A(y,Q^2)}{R_V^A(x,Q^2)} - 1\right]V(y,Q^2),\end{aligned} \tag{19}$$

where we used the expression

$$P_{qq}(z) = \frac{4}{3}\left[\left(\frac{1+z^2}{1-z}\right)_+ + \frac{3}{2}\delta(1-z)\right] \tag{20}$$

for the quark-quark splitting function [24]. The integration gives a finite number at each x, and thus $\partial R_V(x,Q^2)/\partial Q^2 \to 0$ when $x \to 0$.

So, we have been able to show that the three data sets we have used (NMC, SLAC deep inelastic scattering, E772 Drell-Yan production) and our parameterization of the ratio $R^A_{F_2}$ are comparable, and to confirm the results by Qiu. What is *not* reported before, though very probably computed already by Qiu, is the different behavior of the ratio $R^A_G(x,Q)$. As seen in figures 2-4, gluons exhibit a clear diminishing of shadowing when the scale is increased from $Q^2 = 4$ GeV^2 to 100 GeV^2. The conclusion is the same with both Ansätze for gluons we have, both for ^{40}Ca and ^{196}Au: shadowing of gluons vanishes more rapidly than shadowing of quarks and antiquarks. Note that in spite of our somewhat naive initial distributions for gluons, the evolution equations rapidly give us more realistic distributions at higher scales, i.e. we get a rapid rise at $x \sim 1$, and a bump is formated into the mid-x region.

Clearly, based simply on the conservation of momentum and the QCD-evolution in free protons, we can understand the result for gluons: if the ratio R^A_G the mid-x region remains roughly the same at higher scales, and if at the same time more momentum is flowing into gluons from quarks and antiquarks, there *has* to be a rapid rising of the ratio R^A_G in the shadowing region. In fact, we should be able to predict the behaviour of R^A_S and R^A_G already from the usual AP-equations which govern the QCD-evolution, as verified in figs. 4. Let us therefore consider the following case analytically. For simplicity, we consider shadowing of the flavor singlet distribution,

$$\Sigma_A(x,Q^2) = \sum_i \left[q_{i/A}(x,Q^2) + \bar{q}_{i/A}(x,Q^2)\right] = V_A(x,Q^2) + S_A(x,Q^2), \tag{21}$$

and define $R^A_\Sigma(x,Q^2) \equiv \Sigma_A(x,Q^2)/\Sigma(x,Q^2)$. Then, proceeding as in eq. (19) we obtain from the usual AP-equations for gluons

$$\begin{aligned}\frac{Q^2}{R^A_G}\frac{\partial R^A_G}{\partial Q^2} = \frac{\alpha_s}{2\pi}\int_x^1 \frac{dy}{y}\Bigg\{ & zP_{gq}(z)\left[\frac{R^A_\Sigma(y,Q^2)}{R^A_G(x,Q^2)} - 1\right]\frac{y\Sigma(y,Q^2)}{xG(x,Q^2)} \\ & + zP_{gg}(z)\left[\frac{R^A_G(y,Q^2)}{R^A_G(x,Q^2)} - 1\right]\frac{yG(y,Q^2)}{xG(x,Q^2)}\Bigg\}\end{aligned} \tag{22}$$

and for the singlet

$$\frac{Q^2}{R_\Sigma^A}\frac{\partial R_\Sigma^A}{\partial Q^2} = \frac{\alpha_s}{2\pi}\int_x^1 \frac{dy}{y}\left\{zP_{qq}(z)\left[\frac{R_\Sigma^A(y,Q^2)}{R_\Sigma^A(x,Q^2)}-1\right]\frac{y\Sigma(y,Q^2}{x\Sigma(x,Q^2)}\right.$$
$$\left. + 2N_f zP_{qg}(z)\left[\frac{R_G^A(y,Q^2)}{R_\Sigma^A(x,Q^2)}-1\right]\frac{yG(y,Q^2)}{x\Sigma(x,Q^2)}\right\}, \tag{23}$$

where again $z = x/y$. For the sake of argument, let us make the simplifying approximation that at the initial scale $R_G^A(x,Q_0^2) \approx R_\Sigma^A(x,Q_0^2) \approx K_R^A\Theta(x_A - x) + R_A(x)\Theta(x - x_A)$, where x_A is some small value of x after which the ratios are constants, K_R^A is the depth of shadowing in this saturation region, and $R_A(x)$ is some function describing the ratios at larger x's. Let us consider the derivatives at the initial scale $Q^2 = Q_0^2$ and at a region where $x < x_A$. Then we get rid of the δ-functions in P_{qq} and in P_{gg} and eqs. (22) and (23) become simpler,

$$\frac{Q^2}{K_R^A}\frac{\partial R_G^A}{\partial Q^2}\bigg|_{\substack{x<x_A\\ Q=Q_0}} = \frac{\alpha_s}{2\pi}\int_{x_A}^1 \frac{dy}{y}\left[\frac{R^A(y)}{K_R^A}-1\right]\left\{zP_{qq}(z)\frac{y\Sigma(y,Q_0^2)}{xG(x,Q_0^2)} + zP_{gg}(z)\frac{yG(y,Q_0^2)}{xG(x,Q_0^2)}\right\} \tag{24}$$

and

$$\frac{Q^2}{K_R^A}\frac{\partial R_\Sigma^A}{\partial Q^2}\bigg|_{\substack{x<x_A\\ Q=Q_0}} = \frac{\alpha_s}{2\pi}\int_{x_A}^1 \frac{dy}{y}\left[\frac{R^A(y)}{K_R^A}-1\right]\left\{zP_{qq}(z)\frac{y\Sigma(y,Q_0^2)}{x\Sigma(x,Q_0^2)} + 2N_f zP_{qg}(z)\frac{yG(y,Q_0^2)}{x\Sigma(x,Q_0^2)}\right\}. \tag{25}$$

Notice that now the lower limit of the integrations is x_A. The splitting functions are expressed in the '+'-prescription [24], and the integrands vanish at the limit $y \to x_A$ since the term $R^A(y)/K_R^A - 1$ gives zero. In the limit $x \to 0$, at all $y \geq x_A$, the splitting functions behave as follows ($z = x/y$):

$$zP_{gq}(z) \sim 1 + (1-z) \to 2, \quad zP_{gg}(z) \sim \frac{z^2}{1-z} + (1+z^2)(1-z) \to 1,$$
$$zP_{qq}(z) \sim \frac{z(1+z^2)}{1-z} \to 0, \quad zP_{qg}(z) \sim z^3 + z(1-z)^2 \to 0, \tag{26}$$

At the initial scale $xG(x,Q_0^2)$ and $x\Sigma(x,Q_0^2)$ are finite at this limit, and we get the the expected result, $\partial R_G^A/\partial Q^2 \gg \partial R_\Sigma^A/\partial Q^2$ at small x. We thus conclude that already from the unmodified AP-equations one can obtain the result that shadowing for gluons vanishes more rapidly at low values of Q^2 than it does for quarks and antiquarks.

4. Inclusive 1-jet cross sections in pA and AA collisions

As an example of various applications of parton distributions in nuclei, we consider inclusive 1-(mini)jet production in pA and AA collisions at very high energies. The inclusive differential cross section per nuclen-nucleon collision for producing one jet, with transverse momentum $p_{\rm T}$ and rapidity $y = 0$, in a collision of A and B, is given in the lowest order perturbative QCD by the $\hat{u}, \hat{t}$ -symmetrized formula [36]:

$$\left.\frac{d\sigma^{AB}_{\rm jet}}{dp_{\rm T}dy}\right|_{y=0} = \int_{-y_0}^{y_0} dy_2 \frac{2\pi p_{\rm T}}{\hat{s}} \sum_{\substack{ijkl=\\ q,\bar{q},g}} x_1 f_{i/A}(x_1, p_{\rm T}^2) x_2 f_{j/B}(x_2, p_{\rm T}^2) \hat{\sigma}^{ij\to kl}(\hat{s}, \hat{t}, \hat{u}), \quad (27)$$

where, since $y = 0$, the kinematical variables are

$$\begin{aligned} x_{\substack{1\\2}} &= \frac{p_{\rm T}}{\sqrt{s}}(1 + e^{\pm y_2}), \;\; y_0 = \ln(\sqrt{s}/p_{\rm T} - 1), \\ \hat{s} &= x_1 x_2 s, \;\; \hat{t} = -p_{\rm T}^2(1 + e^{-y_2}), \;\; \hat{u} = -p_{\rm T}^2(1 + e^{y_2}). \end{aligned} \quad (28)$$

The hats refer to parton-parton subcollision and $\sqrt{s}$ is the CMS energy of a hadron-hadron subcollision. The cross sections of the eight different subprocess $ij \to kl$ which contribute to the cross section, are denoted by $\hat{\sigma}^{ij\to kl} = \frac{\hat{s}}{\pi}\frac{d\hat{\sigma}}{d\hat{t}}^{ij\to kl}$ and they can be found e.g. in ref. [37]. The number density of a parton i in A is denoted by $f_{i/A}$. The cross section (27) is an average quantity, i.e. it is considered as averaged over the impact parameter between A and B. Cross sections and parton distributions which depend on the impact parameter have been discussed in refs. [38].

We want to express the formula (27) in a form from which we can see the effect of the modification functions, defined as $R_i^A(x, Q^2) \equiv f_{i/A}(x, Q^2)/f_i(x, Q^2)$. Therefore, we divide the integration into negative and positive y_2. In the negative y_2-integrand we change $y_2 \to -y_2$ and use the property $x_{1,2}(-y_2) = x_{2,1}(y_2)$, $\hat{s}(-y_2) = \hat{s}(y_2)$, $\hat{t}(-y_2) = \hat{u}(y_2)$ and $\hat{u}(-y_2) = \hat{t}(y_2)$. Then, by changing the indices $i \leftrightarrow j$, and using $\hat{\sigma}^{ji\to kl}(\hat{s}, \hat{u}, \hat{t}) = \hat{\sigma}^{ij\to kl}(\hat{s}, \hat{t}, \hat{u})$, we get the common factor $\hat{\sigma}^{ij\to kl}(\hat{s}, \hat{t}, \hat{u})$ and eq. (27) becomes

$$\begin{aligned} \left.\frac{d\sigma^{AB}_{\rm jet}}{dp_{\rm T}dy}\right|_{y=0} = \int_0^{y_0} dy_2 \frac{2\pi p_{\rm T}}{\hat{s}} \sum_{\substack{ijkl=\\ q,\bar{q},g}} \Big\{ R_i^A(x_1, p_{\rm T}^2) R_j^B(x_2, p_{\rm T}^2) + R_i^B(x_1, p_{\rm T}^2) R_j^A(x_2, p_{\rm T}^2) \Big\} \cdot \\ \cdot\, x_1 f_i(x_1, p_{\rm T}^2) x_2 f_j(x_2, p_{\rm T}^2) \hat{\sigma}^{ij\to kl}(\hat{s}, \hat{t}, \hat{u}). \end{aligned} \quad (29)$$

It is perhaps illustrative to express the jet production cross section also as an integral over the variable x_1, then we explicitly see which x-range of the parton densities the jet and minijet production probes:

$$\left.\frac{d\sigma_{\rm jet}^{AB}}{dp_{\rm T}dy}\right|_{y=0} = \frac{2\pi}{\sqrt{s}}\int_{x_0}^{1}\frac{dx_1}{x_1^2}\sum_{\substack{ijkl=\\ q,\bar{q},g}}\left\{R_i^A(x_1,p_{\rm T}^2)R_j^B(x_2,p_{\rm T}^2)+R_i^B(x_1,p_{\rm T}^2)R_j^A(x_2,p_{\rm T}^2)\right\}\cdot$$
$$\cdot\, x_1 f_i(x_1,p_{\rm T}^2)x_2 f_j(x_2,p_{\rm T}^2)\hat{\sigma}^{ij\to kl}(\hat{s},\hat{t},\hat{u}), \tag{30}$$

where $x_0 = 2p_{\rm T}/\sqrt{s}$ and $x_2 = x_1/(x_1\sqrt{s}/p_{\rm T}-1)$.

Most of the cross section (30) is due to the gluonic subprocess $gg \to gg$. Obviously, the differential cross section is also peaked around $x_1 \sim x_2 \sim x_0$. Since x_2 changes in eq. (30) from x_0 to $1/(\sqrt{s}/p_{\rm T}-1) \approx p_{\rm T}/\sqrt{s}$, gluons at x_2 come always from the shadowing region, if $p_{\rm T}$ is sufficiently low and $\sqrt{s}$ high. Therefore, it would be a tempting idea to use jet production to measure shadowing of gluons also. However, if the results of this paper are correct, as we expect, the scale evolution of gluon distributions seems to make it rather unlikely that jet production in pA or in AA could be used for that purpose at $\sqrt{s} \sim 200$ GeV. This is indicated in figs. 5, where we show the cross section (30) versus $p_{\rm T}$ at $\sqrt{s} = 200$ GeV in the two scenarios we have for gluons.

Let us consider more closely jet production in for example pA collisions. In eq. (30) we substitute $R_g^B = 1$. In the minijet production region ($p_{\rm T} \sim p_0 \sim 2$ GeV) the effect of shadowing could be seen if one were able to detect the minijets. Unfortunately, already in pp collisions it is hard to find any jets below $p_{\rm T} < 5$ GeV due to large multiplicities [7], and in case of a nucleus the situation is even worse. In fig. 7 we have illustrated the effect of increasing $p_{\rm T}$ of jets. The diamonds (triangles) mark the lowest values of x_1 in the integration of eq (30) at at each $Q = p_{\rm T}$, and at the same time the regions where the integrand in (30) is peaked (larger x_1's contribute also, since we have to integrate over all x_1's). Moving towards larger $p_{\rm T}$ increases x's as well, as seen in the figure. We see that for $\sqrt{s} = 200$ GeV, even if gluons at $Q = p_{\rm T} = p_0$ are strongly shadowed, the *observable* jets with $p_{\rm T} \gtrsim 5$ GeV are practically *not* anymore suppressed. This is reflected to the ratio of the cross sections in fig. 5a and b. In AA experiments the transverse momenta of observable jets are most probably higher than 5 GeV, which means that we move further away from the shadowing region of gluons.

For $\sqrt{s} = 6500$ GeV, see fig. 6, the situation may be different, since then typically $x \sim 0.0015$ when $p_T \sim 5$ GeV, and gluons should still be clearly shadowed (see also figs 2-4 and 7). Unfortunately enough, at the LHC one will not be able to do pA experiments. A word of caution is perhaps appropriate in here. A bold extrapolation from $\sqrt{s} = 200$ GeV to 6500 GeV by using Duke-Owens distributions and the ratios

of figs. 2-3 may not be quite correct: at *extremely small* x one expects shadowing of gluons to take place already in protons [39]. However, at $\sqrt{s} = 200$ GeV we are mainly not probing such small x's, and hence the prediction presented here is more reliable for the RHIC energies.

As a conclusion, we state that unless gluons are a lot more shadowed than in our Ansatz 2 (fig. 3a), it will most probably be very difficult to measure shadowing of gluons with the inclusive 1-jet production in pA or in AA at $\sqrt{s} = 200$ GeV. Consequently, we would like to stress that even if one would not observe any shadowing (of gluons)via the jet production at RHIC (or even at LHC), one should not draw the conclusion that there would not be a possibly strong shadowing of gluons at lower momentum scales.

5. Discussion

In this paper, we have studied QCD-evolution of parton distributions in heavy nuclei with distributions constrained to conserve both baryon charge and momentum. The parton distributions at an initial scale $Q_0 = 2$ GeV were further constrained by the available data on $\frac{1}{A}F_2^A/\frac{1}{2}F_2^D$, from deep inelastic lepton-nucleus collisions [14,10] and by the data on the anti(sea)quarks from the Drell-Yan lepton pair production in proton-nucleus collisions [17]. For the gluon distributions, we considered two different Ansätze for gluon shadowing. The QCD-evolution was then computed using the Altarelli-Parisi-equations [24], modified by terms calculated by Mueller and Qiu [16]. The main conclusion in each case is the same: gluon shadowing vanishes much more rapidly than that of quarks and antiquarks. In addition, the greater the gluon shadowing, the slower does the shadowing of seaquarks vanish. This confirms the results of Qiu [15]. The slow Q^2 dependence in the ratio $\frac{1}{A}F_2^A/\frac{1}{2}F_2^D$ is in accord with the experimental observations [13,14], especially also at small values of x and 4 GeV$^2 \lesssim Q^2 \lesssim 10$ GeV^2.

We recall the underlying approximations in the present analysis. In analyzing the deep inelastic scattering data [14,10], we assumed that the ratio of absorption cross sections of longitudinally and transversally polarized virtual photons does not depend on the target. With this approximation the ratio $\frac{1}{A}F_2^A/\frac{1}{2}F_2^D$ is directly given by the ratio of differential deep inelastic lepton-nucleon scattering cross sections in A and D [14]. We neglect the target-mass corrections [23], and small shadowing effects in D as well [26]. We also assume that, in the first approximation, seaquarks and sea antiquarks have the same nuclear distributions. Since the net charge and strangeness of sea has to vanish, we do not expect corrections to this to be significant. The difference between

the distributions of quarks and antiquarks in nuclei would nevertheless be interesting to look at [25]. As stated in section 2, our initial distributions were construct to conserve the baryon charge within 3.5 % in a wide range of nuclei, from $A = 12$ to $A = 196$. We neglected the few per cent corrections due to different numbers of protons and neutrons in non-isoscalar nuclei. For our purposes, more accurate error analysis is not needed here, since the main uncertainty comes from the gluons, especially from the unknown gluon shadowing part.

What was not discussed here at all, though potentially an important subject in heavy nuclei, was the effect of nuclear geometry to the parton densities: nuclear parton structure is most likely different in the center of the nucleus than in peripheral regions [38]. Inclusion of nuclear geometry is not necessarily an easy task, since different x-regions require different treatments, and also the QCD-evolution is affected by the geometry.

Next, we comment on some observational consequences of the nuclear parton, especially gluon, distributions. Inclusive (mini)jet production was discussed in section 4. We found (figs. 5) that the observable jets at RHIC are influenced by the antishadowing region. However, the present analysis indicated that gluon antishadowing is likely to remain small, $\lesssim 20$ % even for the extreme anSatz 2 considered here.

Of course, 2-3 GeV minijets may be quite strongly affected by the gluon shadowing already at RHIC energies. This reduces the pre-equilibrium energy densities (see e.g. [38,3,4]) and lowers the initial temperature of the system. Because of shadowing there are fewer semihard gluons formed, and thermalization of the gluon-quark-system may also be slowered [40], which lowers the initial temperature as well. A high initial temperature is important for production of thermal photons and dileptons, which are one of the suggested signatures of quark-gluon plasma [6]. Thermal rates must be compared to the background, which at transverse momenta $p_{\mathrm{T}} \gtrsim 2$ GeV is dominantly due to the primary (pre-equilibrium) hard collisions. Hard collisions are sensitive to the changes of the scale in the nuclear parton densities (see fig. 7), especially when gluons are involved, e.g. depletion due to gluon shadowing in the direct photon rates will decrease with inreasing p_{T}. It will be interesting to study to what extent the scale dependence of gluon shadowing affects the possibility of observing thermal photons and dileptons.

As seen in figs. 2 and 3, the depth of gluon shadowing affects the rate with which shadowing in sea(anti)quarks and in the F_2-ratio is decreasing when evolving towards larger Q^2. If it were possible to measure accurately enough the scale dependence of $R^A_{F_2}$ and R^A_S at fixed x, one could constrain the amount of the gluon shadowing at $Q_0 = 2$ GeV. For instance, in pA collisions at RHIC energies the differences in Drell-Yan dilepton production at large x_{F} (corresponds to small x_2) at different fixed scales

$Q = M$, from 2 GeV to 10 GeV, should tell whether the gluons are strongly shadowed (relatively small difference between $R_S^A(x, M^2 = 4\ \mathrm{GeV}^2)$ and $R_S^A(x, M^2 = 100\ \mathrm{GeV}^2)$, see fig. 3) or moderately shadowed (larger difference). However, it may be difficult to get high enough dilepton statistics to make such a precision measurement. Of course, before this, one must also include a proper analysis of the QCD-correctios to the Drell-Yan cross sections [41] to carry out such a program.

As discussed in [22], gluon shadowing can be studied via production of heavy quark bound states, J/Ψ, Ψ' and Υ. If done so, especially if we wish to compare J/Ψ and Υ production cross sections in pA collisions at very high energies (low values of x_2), the scale dependence of nuclear gluon structure has to be taken into acount. If the final state interactions of these bound states could be computed [42], and if their effect could be subtracted, then one could obtain information on the gluon densities at scales $Q_\psi \sim M_\Psi \sim 3$ GeV and $Q_\Upsilon \sim M_\Upsilon \sim 10$ GeV. For instance, in the case of Υ one has to do backwards scale evolution down to $Q \sim 3$ GeV and only then compare the obtained gluon distributions.

We believe we have now been able to shed some light on the problem of gluon structure in heavy nuclei, at least on the behaviour with increasing scales. Clearly, from the point of view of perturbative processes, the most important and urgent improvement to the present analysis is a reliable determination of gluon shadowing at low (initial) values of the scale Q.

Acknowledgements:

I would like to thank Miklos Gyulassy for suggesting the study of this subject as well as for several helpful discussions. I also wish to thank Xin-Nian Wang and Sourendu Gupta for correspondence and for motivating discussions. Finally, I would like to thank the Academy of Finland, Emil Aaltonen foundation and Magnus Ehrnrooth foundation for financial support.

Appendix

A. Parameterization of the ratio $\frac{1}{A}F_2^A/\frac{1}{2}F_2^D$

We parameterize the deep inelastic lepton scattering data [14,10] for the ratio $R_{F_2}^A = \frac{1}{A}F_2^A/\frac{1}{2}F_2^D$ in the following way:

$$
\begin{aligned}
R_{F_2}^A = 1 & \\
& - K(A^{1/3}-1)\left\{e^{-(x/x_A)^{1.2}} + (1-e^{-(x/x_A)^{1.2}})^{1.4} a_s \frac{\ln(x/x_s^A)}{\ln(x_A/x_s^A)}\right\} e^{-(x/x_{0s})^2} \\
& + \left\{(a_0-1) + a_1 x + a_2 x^2 + a_3 x^3\right\}(1-e^{-(x/x_{0e})^2})\Theta(x_m - x) \\
& + \Theta(x-x_m)\left\{(1-f_m)\left[(x-x_m)/(x_{\mathrm{Fm}}-x_m)\right]^2 + (f_m-1)\right\},
\end{aligned}
\tag{A1}
$$

i.e. we divide the x range basically into three regions: shadowing at $x < x_{0s}$, EMC-effect at $x_{0e} < x < x_m$ and Fermi motion at $x_m < x < 1$. The exponentials play the role of smooth Θ-functions here.

In the shadowing region, we assume the corrections to unity to be mainly from two-parton interactions and we expect the correction to vanish in the case of $A = 1$, hence the scaling $A^{1/3}-1$ [15]. This picture does probably not hold down to extremely low x's [16] but gives us pretty good first approximation to start with. We also expect a saturation of shadowing at $x < x_A$, and we assume that $x_A = x_{\mathrm{Ca}}(A/40)^{-(1/3)}$. In the infinite momentum frame in this picture saturation is motivated when x gets so small that the partonic wavelength exceeds the Lorentz contracted size of the nucleus, and this results the $A^{-(1/3)}$-scaling [15] (for alternative suggestions, see [18-19]). We use $x_{\mathrm{Ca}} = 0.004$, since the NMC data [14] does not show any signs of saturation at larger x's for $A = 40$. Then, the exponentials in eq. (A1) will help to give us both saturation and a smooth change into linear (at log-scale) behaviour. We do not expect the shadowing corrections to be important at $x > x_{0s}$, and we also fix $x_{0s} = 0.13$. The parameter x_s^A describes the point where the shadowing correction disappears, and, based on ref. [43], we write $x_s^A = x_s^{\mathrm{Ca}} k(40)/k(A)$, where the function $k(A) = 1 + 3(2A^{-(1/3)}) - 3(2A^{-(1/3)})^2 + (2A^{-(1/3)})^3$. The physical idea behind this is that the effective distance between two nucleons is shortened because of the nucleons located in the surface of the nucleus. Therefore one expects shadowing at slightly larger x for larger nuclei. This effect, however, is very small. The remaining three parameters, K, a_s and x_s^{Ca}, we determine by minimizing the sum of χ^2's of the shadowing region of the NMC data for isoscalar targets $A = 12$ and $A = 40$. In this way we obtain: $K \approx 1.06(1.065)$, $a_s \approx 0.86(0.857)$ and $x_s^{\mathrm{Ca}} \approx 0.072(0.0717)$.

In the EMC region, $x_{0e} < x < x_m$, we fit simply a third order polynomial $f(x) = a_0 + a_1 x + a_2 x^2 + a_3 x^3$ to the quite extensive data of ref. [10]. We impose the following conditions for the fit $f(x)$:

$$f(x_e) = f_e, \quad f(x_m) = f_m, \quad f'(x_m) = 0, \quad f'(x_{0e}) = 0.$$

Based on the data over the wide range of nuclei [10], we fix $x_e \approx 0.3$ and $f_e = 1.0$, $x_{0e} = 0.12$, and the location of the minimum to $x_m \approx 0.7$ for all A. Depth of the minimum at x_m depends on A, and we find, again by minimizing the χ^2 in the EMC region, that $f_m \approx 0.86(A/40)^{-0.044}$ gives reasonable description of the A scaling in this region.

For our purposes the Fermi motion region at $x > x_m$ is completely uninteresting since practically it does dot contain much momentum or baryon charge. Therefore we simply fix $x_{\mathrm{Fm}} \approx 0.84$ for all A, which is the point where the correction to unity vanishes at large x. The simple parabolic fit coincides smoothly to the polynomial fit at the minimum x_m.

References

[1] L. Durand and H. Pi, Phys. Rev. Lett. 58 (1987) 303.

T. K. Gaisser and F. Halzen, Phys. Rev. Lett. 54 (1985) 1754.

[2] X.-N. Wang, Phys. Rev. D43 (1991) 104, and references therein.

[3] X.-N. Wang and M. Gyulassy, Phys. Rev. D44 (1991) 3501; Phys. Rev. D45 (1992) 844; Phys. Rev. Lett. 68 (1992) 1480.

[4] K. Kajantie, P. V. Landshoff and J. Lindfors, Phys. Rev. Lett. 59 (1987) 2517.

K. J. Eskola, K. Kajantie and J. Lindfors, Nucl. Phys. B323 (1989) 37.

[5] K. J. Eskola, K. Kajantie and J. Lindfors, Phys. Lett. B214 (1989) 613;

E. Shuryak, preprint SUNY-NTG-91-48;

T. S. Biró, B. Müller and X. N. Wang, Duke preprint DUKE-YH-92-26.

[6] R. C. Hwa and K. Kajantie, Phys. Rev. D32 (1985) 1109;

K. Kajantie and P. V. Ruuskanen, Z. Phys. C44 (1989) 167, and references therein;

P. V. Ruuskanen in *Quark Gluon Plasma Signatures*, Éditions Frontiéres 1991, ed. V. Bernard *et al.*;

J. Kapusta, L. McLerran and D. K. Srivastava, University of Minnesota preprint, February 1992, TPI-MINN-92/3-T.

[7] UA1 collaboration, C. Albajar *et al.*, Nucl. Phys. B309 (1988) 405.

[8] EM Collaboration, J.J. Aubert *et al.*, Phys. Lett. B123 (1983) 275.

[9] A. Bodek *et al.*, Phys. Rev. Lett. 50 (1983) 1431; 51 (1983) 534.

[10] R. G. Arnold *et al.*, Phys. Rev. Lett. 52 (1984) 727.

[11] BCDMS Collaboration, G. Bari *et al.*, Phys. Lett. B163 (1985) 282.

[12] EM Collaboration, J. Ashman *et al.*, Phys. Lett. B202 (1988) 603; M. Arneodo *et al.*, Phys. Lett. B211 (1988) 493.

[13] EM Collaboration, M. Arneodo *et al.*, Nucl. Phys. B333 (1990) 1.

[14] NM Collaboration, P. Amaudruz *et al*, Z. Phys. C51 (1991) 387.

[15] J. Qiu, Nucl. Phys. B291 (1987) 746.

[16] A. H. Mueller and J. Qiu, Nucl. Phys. B268 (1986) 427.

[17] D.M. Alde *et al.*, Phys. Rev. Lett. 64 (1990) 2479.

[18] L. L. Frankfurt, M. I. Strikman and S. Liuti, Phys. Rev. Lett. 65 (1990) 1725.

[19] L. L. Frankfurt and M.I. Strikman, Phys. Rep. 160 (1988) 237;
L. L. Frankfurt and M. I. Strikman, Nucl. Phys. B316 (1989) 340.

[20] F. E. Close, J. Qiu and R.G. Roberts, Phys Rev. D40 (1989) 2820.

[21] J. Kwieciński, Z. Phys. C45 (1990) 45.

[22] S. Gupta and H. Satz, CERN Preprint CERN-TH.6400/92.

[23] H. Georgi and H.D. Politzer, Phys. Rev. D14 (1976) 1829.

[24] G. Altarelli and G. Parisi, Nucl. Phys. B126 (1977) 298.

[25] We thank X.-N. Wang for pointing this out, see also ref. [30].

[26] J. Kwieciński and B. Badelek, Warsaw University Preprint IFD/3/1991.

[27] N. N. Nikolaev and V. I. Zakharov, Phys. Lett. B55 (1975) 397.

[28] V. I. Zakharov, Torino Preprint DFTT-10/92, and references therein.

[29] P. Castorina and A. Donnachie, Z. Phys. C45 (1989) 141.

[30] S. J. Brodsky and H. J. Lu, Phys. Rev. Lett. 64 (1990) 1342.

[31] F. E. Close, R. G. Roberts and G. G. Ross, Phys. Lett. B129 (1983) 346;
R. L. Jaffe *et al.*, Phys. Lett. B134 (1984) 449.

[32] D. W. Duke and J. F. Owens, Phys. Rev. D30 (1984) 49.

[33] T. Sjöstrand and M. van Zijl, Phys. Rev. D36 (1987) 2019;
N. Abou-El-Naga, K. Geiger and B. Müller, Duke preprint DUKE-TH-91-19.
[34] D. M. Alde *et al.*, Phys. Rev. Lett. 66 (1991) 133.
[35] NA3 Collaboration, J. Badier *et al.*, Z. Phys C20 (1983) 101.
[36] S. Ellis and M. Kislinger, Phys. Rev. D9 (1974) 2027.
[37] I. Sarcevic, S. D. Ellis and P. Carruthers, Phys. Rev. D40 (1989) 1446.
[38] K. J. Eskola, Z. Phys. C51 (1991) 633.
P. Castorina and A. Donnachie, Z. Phys. C49 (1991) 481.
[39] J. Kwieciński et al., Phys. Rev. D42 (1990) 3645.
[40] K.J. Eskola and M. Gyulassy, under preparation.
[42] S. Gavin, M. Gyulassy and A. Jackson, Phys Lett B207 (1988) 257;
S. Gavin and R. Vogt, Nucl. Phys. B345 (1990) 104.
[41] G. Altarelli, R. K. Ellis and G. Martinelli, Nucl. Phys. B157 (1979) 461.
[43] E. L. Berger and J. Qiu, Phys. Lett. B206 (1988) 141.

Figure captions

Figs. 1 a,b. The ratios of the parton distributions in a nucleus A to the ones in deuteron (a: ^{12}C, b: ^{40}Ca) at an initial scale $Q = Q_0 = 2$ GeV, as defined in eqs. (5) and (8). Only our 'Ansatz 1' is shown for gluon ratio R_G^A (solid line). The data points shown are the deep inelastic NMC 200 GeV μA data [14] (diamonds) and the SLAC 8-24.5 GeV eA data [10] for the ratio $R_{F_2}^A$ (crosses), and the E772 800 GeV pA Drell-Yan data [17] corresponding to the ratio R_S^A (boxes). The parameterization (A1) of $R_{F_2}^A$ is plotted with a dashed line. Valence quarks, R_V^A, are shown by the dotted line, and seaquarks, R_S^A by the dotted-dashed line.

Fig. 2 a,b,c. Scale evolution of the ratios $R_G^A(x,Q^2)$, $R_V^A(x,Q^2)$, $R_S^A(x,Q^2)$ and $R_{F_2}^A(x,Q^2)$ for $A = 196$, as predicted by the modified Altarelli-Parisi equations [16] of eqs (12-14). The ratios are shown as functions of x at scales $Q = 2$, 3, 5, 7, and 10 GeV, which are indicated on the respective curves. The initial distributions at $Q = 2$ GeV are obtained by using our parameterization (A1) with $A = 196$ and neglecting small corrections due to the non-isoscalarness (cf. eq. (5)) and the procedure described in sec. 2. The initial distribution for gluons in fig. 2a is our **Ansatz 1**. The data shown is the deep inelastic SLAC 8-24.5 GeV eA data [10] for the ratio $R_{F_2}^A$(crosses), and the E772 800 GeV pA Drell-Yan data [17] for the ratio R_S^A (boxes). Notice 1) that the evolution of $R_{F_2}^A$ from $Q = 2$ GeV to $Q = 3$ GeV is slow [15], and thus coincides with the nonvanishing of shadowing observed at small scales in the deep inelastic data for ^{40}Ca [14], 2) that the shadowing of gluons vanishes much more rapidly than the shadowing of quarks and antiquarks.

Fig. 3 a,b,c. The same as figs. 2 but with gluons in the **Ansatz 2** at the initial scale $Q = 2$ GeV. The data shown in fig. 3a is the E772 800 GeV pA data for J/Ψ (diamonds) and Ψ' (boxes) production [34] and the NA3 200 GeV πPt (triangles), 200 GeV πPt ($\times$) and 200 GeV pPt (+) for J/Ψ production [35], as plotted in ref. [22]. Here the evolution of sea, and hence $R_{F_2}^A$ is clearly slower than with the gluons of 'Ansatz 1': the stronger shadowing of gluons is reflected to the behavior of R_S^A since the evolution equations (13) and (14) are coupled.

Fig. 4 a,b,c. The same as figs. 3 a,b,c but with the scale evolution given by the traditional Altarelli-Parisi-terms only (eqs. (12-14) without the modifications). By comparing figs. 3 and 4 we see that the mainline of QCD-evolution is determined by the unmodified Altarelli-Parisi equation; the Mueller-Qiu modifications give then the corrections to this evolution by slowering down the relative evolution of partons [15,16].

Fig. 5 a,b. The average inclusive one-jet cross sections per nucleon-nucleon collision in pp, pA and AA collisions at $\sqrt{s} = 200$ GeV with $A = 196$ and $y = 0$, plotted as a function of the transverse momentum p_T of a jet, computed from eq. (27). The data shown is the minijet data of UA1 collaboration from $p\bar{p}$ collisions at

$\sqrt{s} = 200$ GeV [7]. **c, d.** The ratio of the pA and AA one-jet cross sections to pp one-jet cross section versus p_T. a and c: Ansatz 1, b and d: Ansatz 2 for gluons. For the parton distributions in a free proton we used Duke-Owens set 1 [32] with $\Lambda_{QCD} = 200$ MeV. K-factor $K = 2$ was also used, this is cancels out in figs c and d.

Fig. 6. The same as in fig. 5 but for $\sqrt{s} = 6500$ GeV.

Fig. 7. An illustration of what region of the gluon ratio $R_G^A(x, Q^2)$ the inclusive one-jet production, eqs. (27-30), probes. The diamonds (triangles) are the lower limits of integration in eq. (30) for $\sqrt{s} = 200$ (6500) GeV and at the same time the x-values into which the integrands are peaked at each $Q = p_T$. The lines shown are only for guiding the eye and for showing how the shadowing of gluons vanishes when p_T is increased.

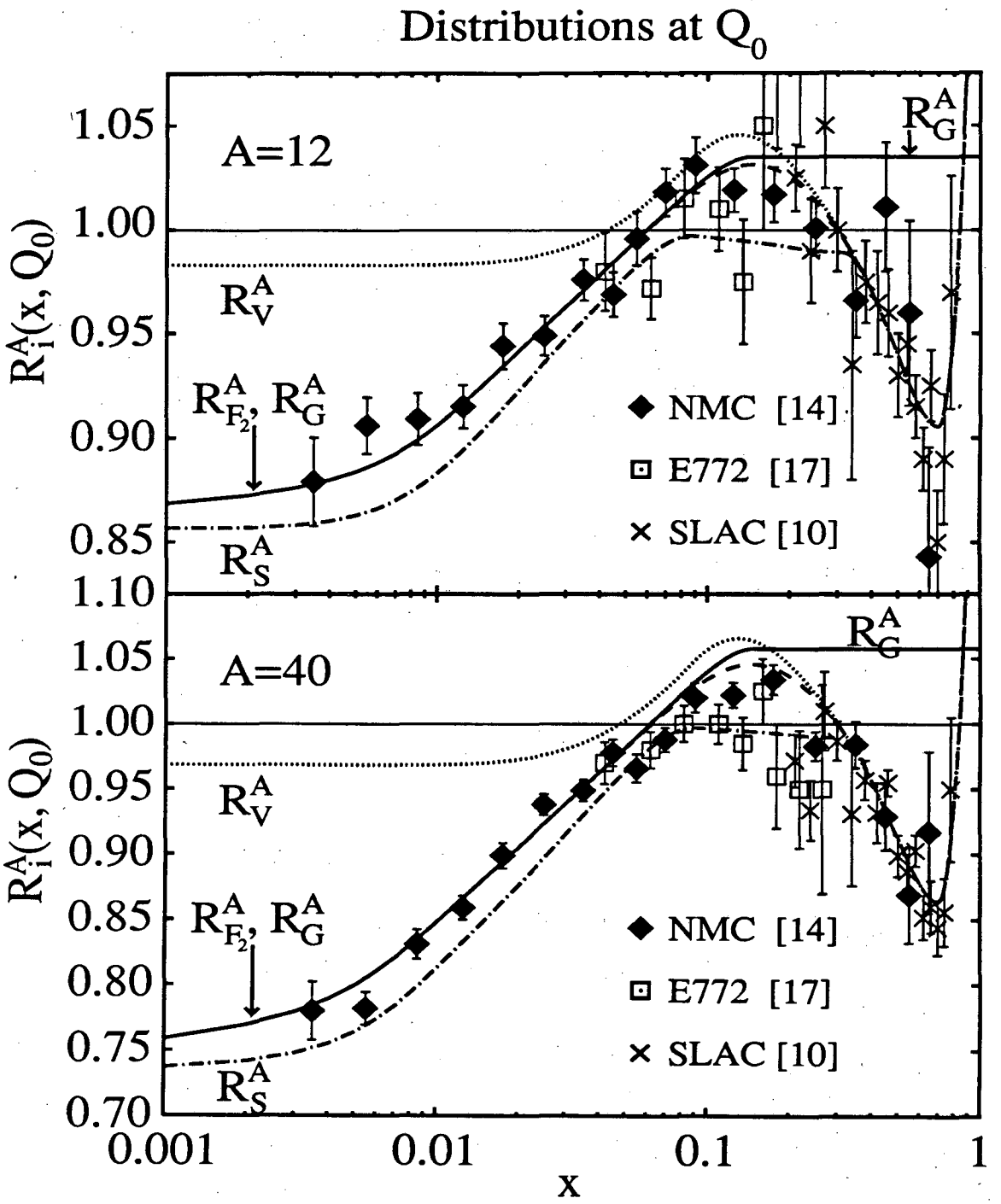
Distributions at Q_0
A=12
A=40
$R_i^A(x, Q_0)$
R_V^A
R_S^A
R_G^A
$R_{F_2}^A$, R_G^A
NMC [14]
E772 [17]
SLAC [10]
1.05
1.00
0.95
0.90
0.85
1.10
0.80
0.75
0.70
0.001
0.01
0.1
1
x

Fig. 1

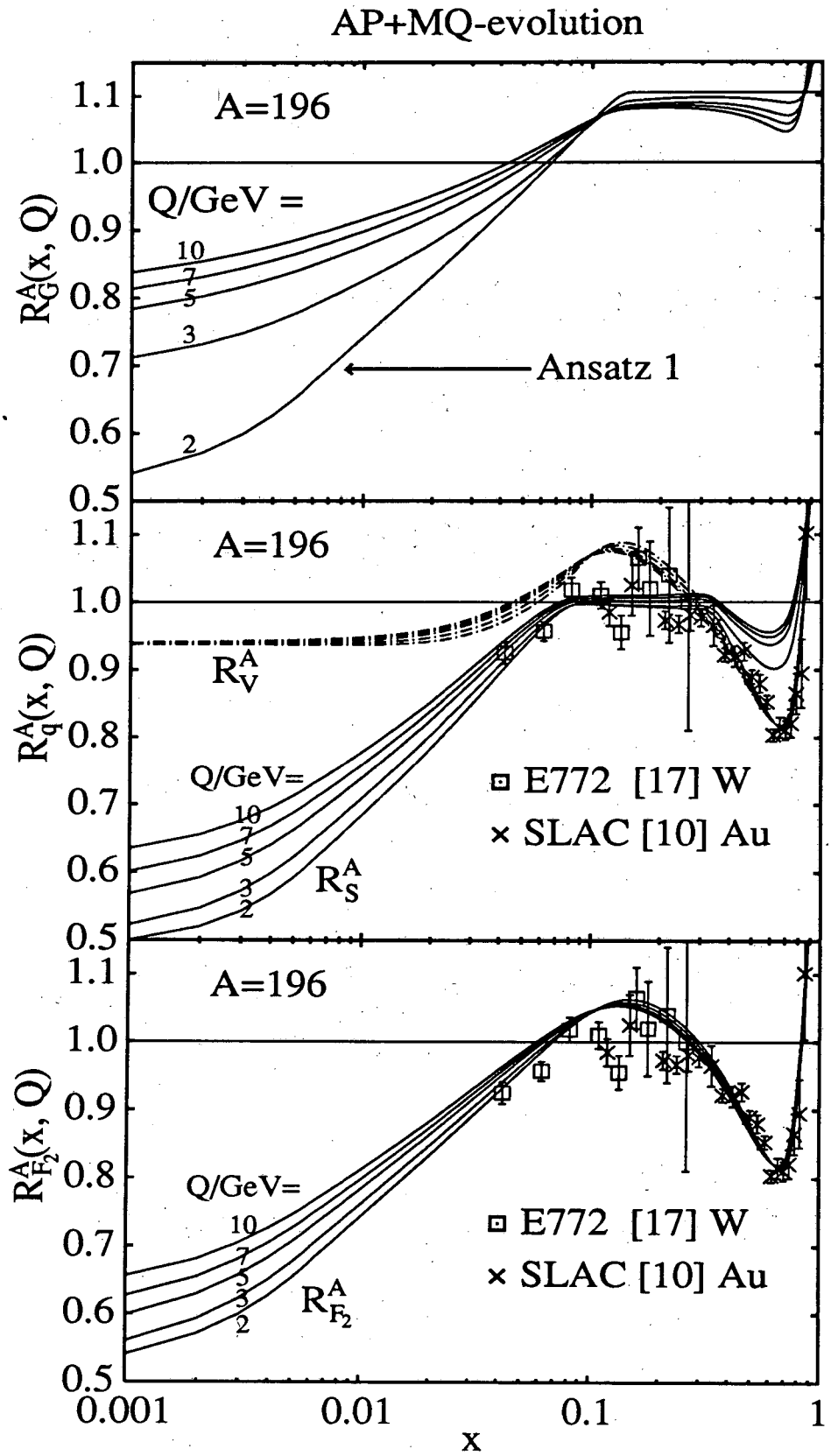
AP+MQ-evolution
A=196
Q/GeV =
10
7
5
3
2
Ansatz 1
$R_G^A(x, Q)$
A=196
R_V^A
Q/GeV=
10
7
5
3
2
R_S^A
E772 [17] W
SLAC [10] Au
$R_q^A(x, Q)$
A=196
Q/GeV=
10
7
5
3
2
$R_{F_2}^A$
E772 [17] W
SLAC [10] Au
$R_{F_2}^A(x, Q)$
1.1
1.0
0.9
0.8
0.7
0.6
0.5
0.001
0.01
0.1
1
x

Fig. 2

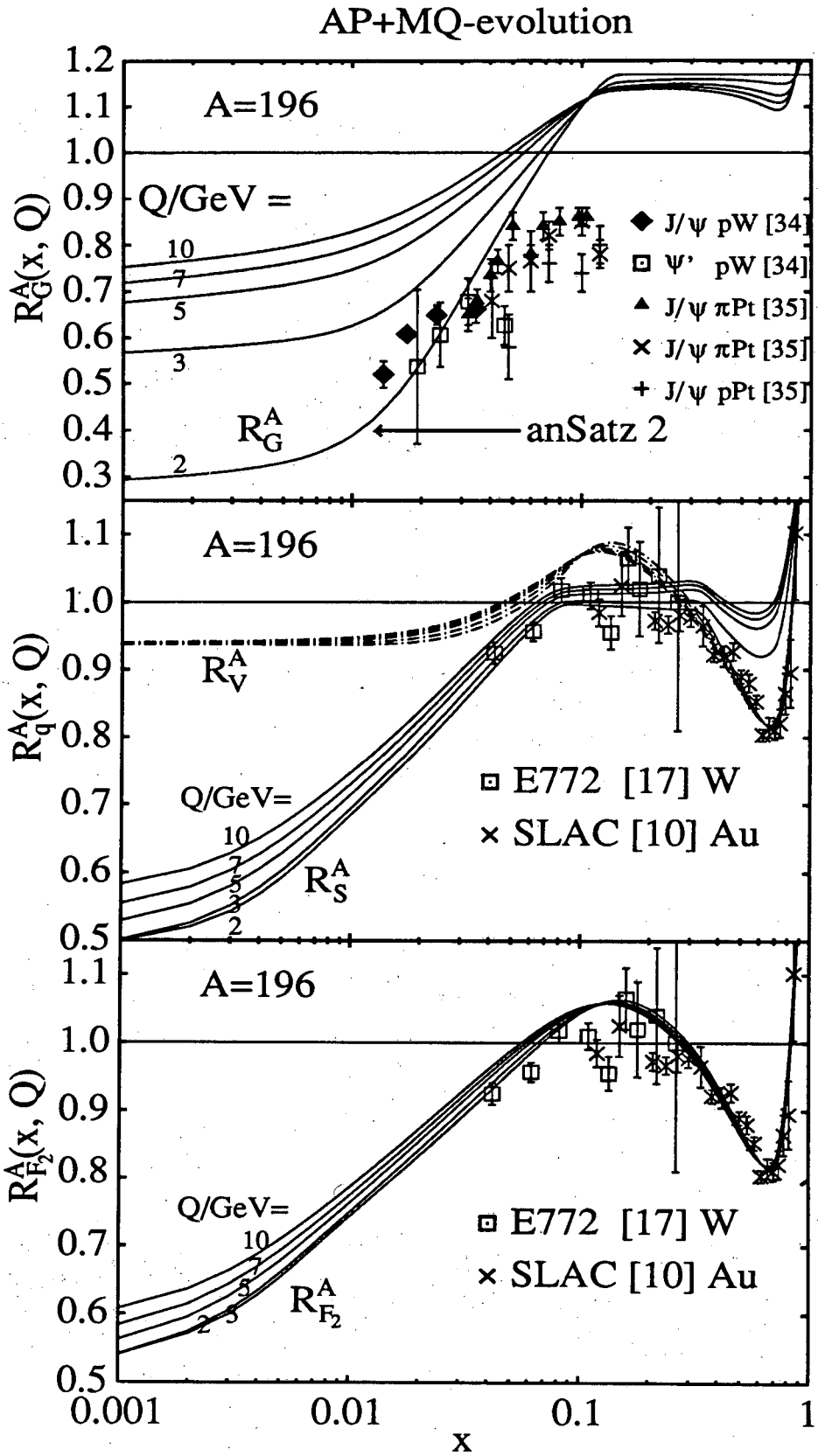
AP+MQ-evolution
A=196
Q/GeV =
10
7
5
3
2
R_G^A
anSatz 2
J/ψ pW [34]
ψ' pW [34]
J/ψ πPt [35]
J/ψ πPt [35]
J/ψ pPt [35]
$R_G^A(x, Q)$
A=196
R_V^A
R_S^A
Q/GeV=
E772 [17] W
SLAC [10] Au
$R_q^A(x, Q)$
A=196
$R_{F_2}^A$
Q/GeV=
E772 [17] W
SLAC [10] Au
$R_{F_2}^A(x, Q)$
0.001
0.01
0.1
1
x

Fig. 3

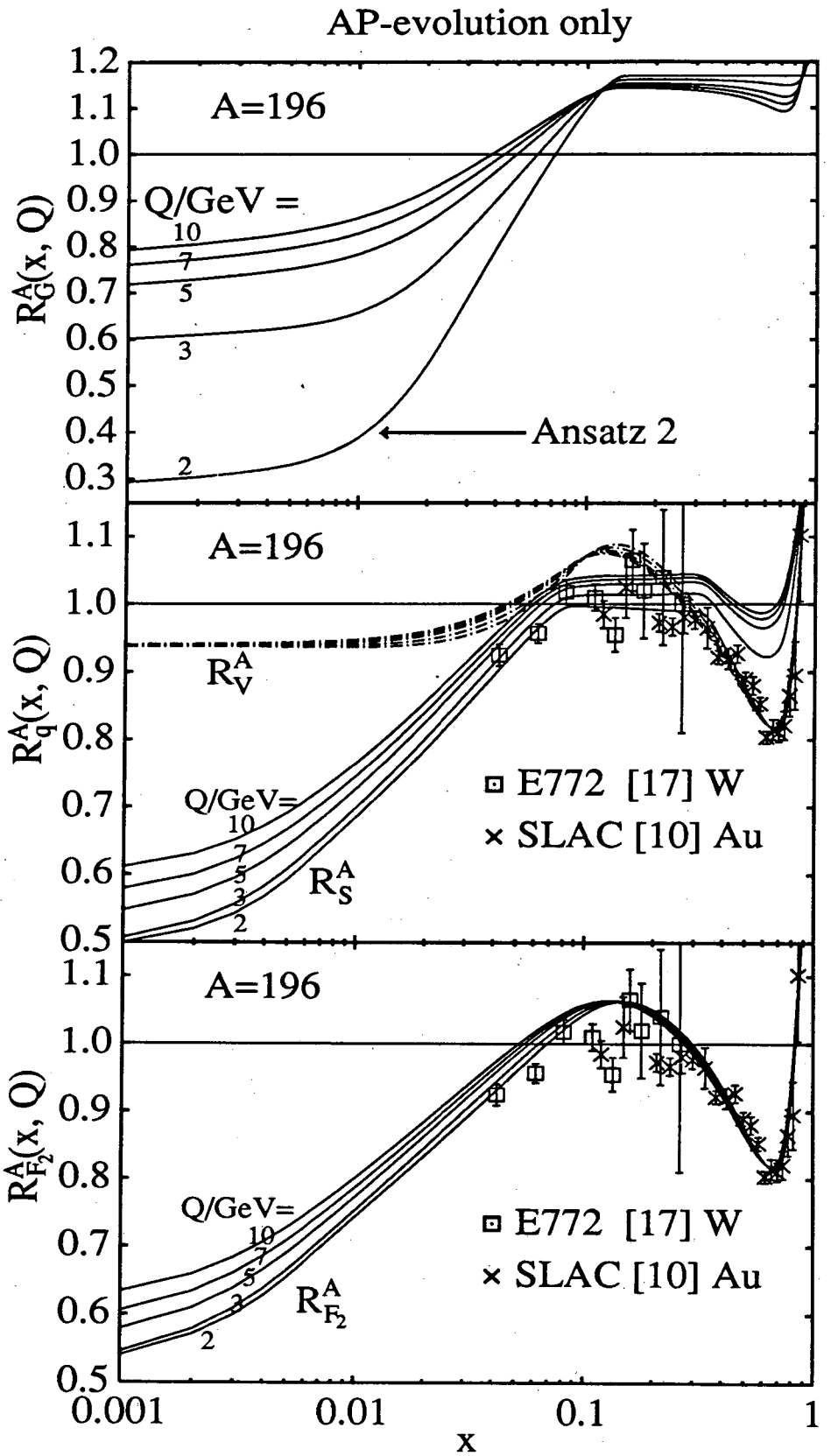
AP-evolution only
A=196
Q/GeV =
10
7
5
3
2
Ansatz 2
$R_G^A(x, Q)$
A=196
R_V^A
R_S^A
Q/GeV=
E772 [17] W
SLAC [10] Au
$R_q^A(x, Q)$
A=196
$R_{F_2}^A$
Q/GeV=
E772 [17] W
SLAC [10] Au
$R_{F_2}^A(x, Q)$
x

Fig. 4

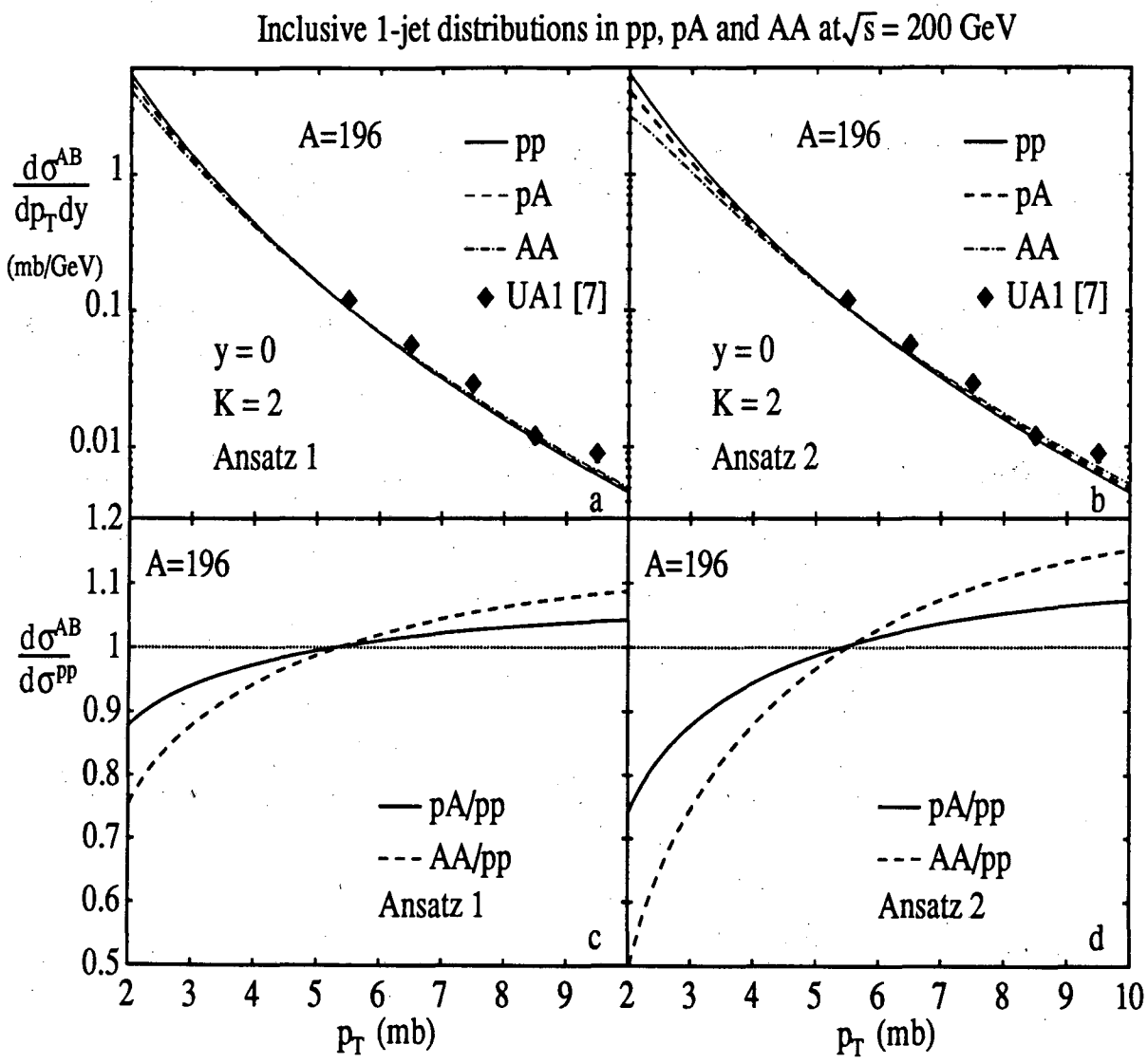
Inclusive 1-jet distributions in pp, pA and AA at $\sqrt{s}$ = 200 GeV
$\frac{d\sigma^{AB}}{dp_T dy}$ (mb/GeV)
A=196
pp
pA
AA
UA1 [7]
y = 0
K = 2
Ansatz 1
Ansatz 2
a
b
$\frac{d\sigma^{AB}}{d\sigma^{pp}}$
pA/pp
AA/pp
c
d
p_T (mb)

Fig. 5

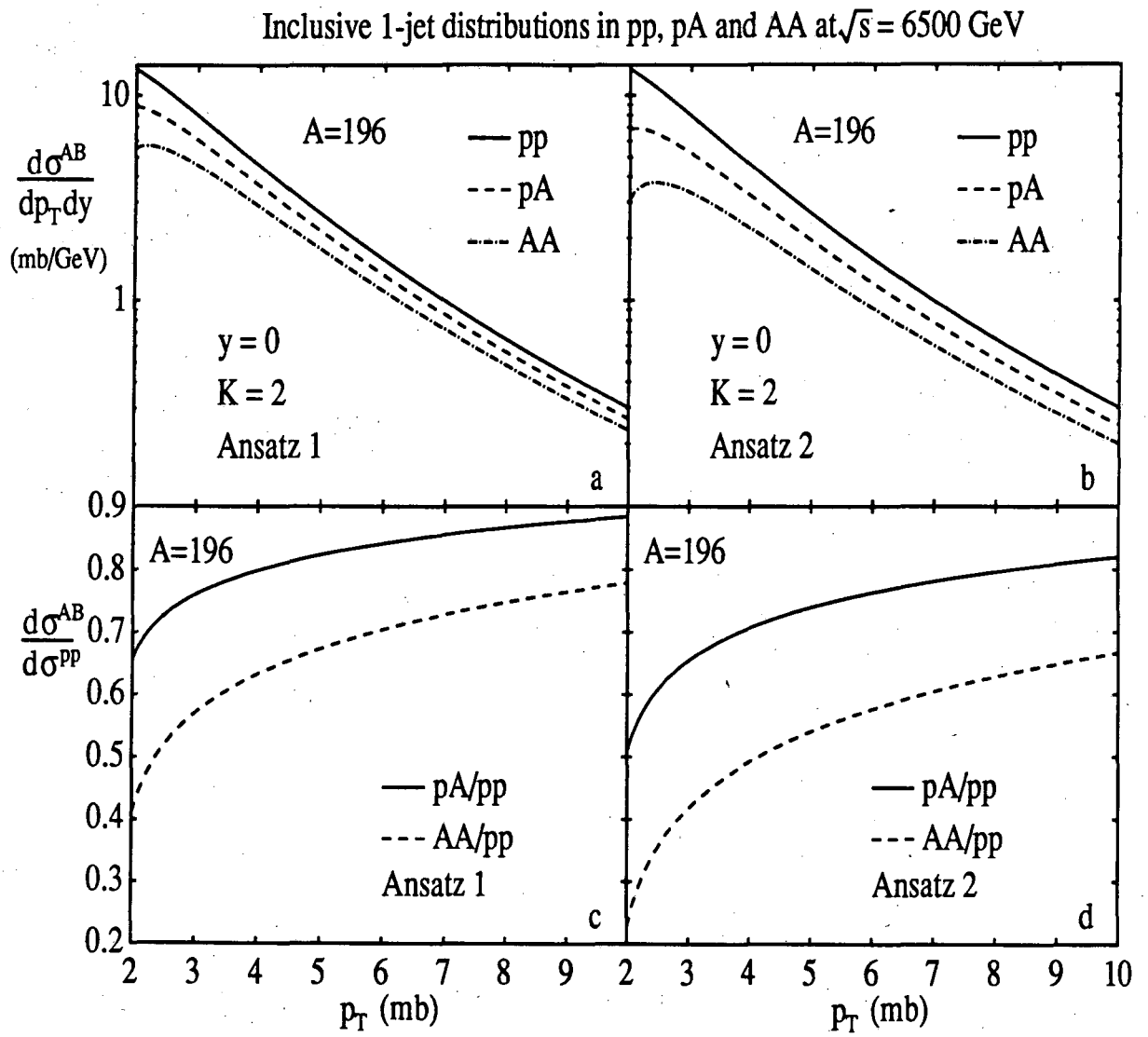
Inclusive 1-jet distributions in pp, pA and AA at $\sqrt{s}$ = 6500 GeV
$\frac{d\sigma^{AB}}{dp_T dy}$ (mb/GeV)
A=196
pp
pA
AA
y = 0
K = 2
Ansatz 1
a
Ansatz 2
b
$\frac{d\sigma^{AB}}{d\sigma^{pp}}$
pA/pp
AA/pp
c
d
p_T (mb)

Fig. 6

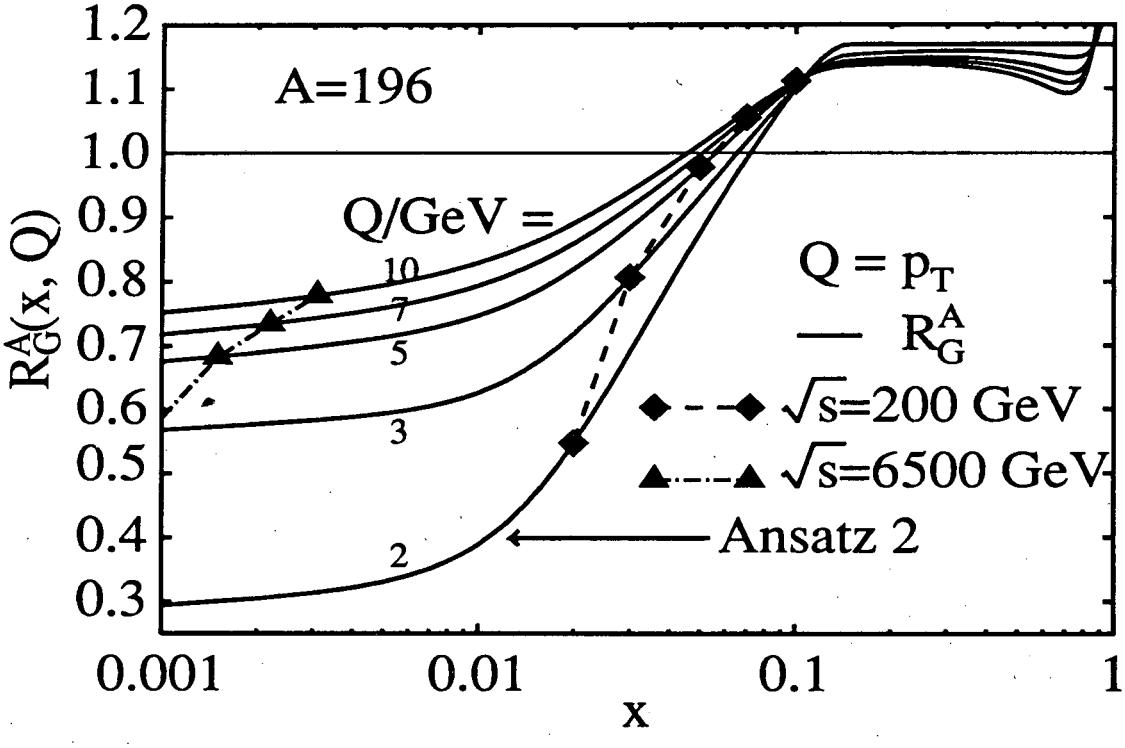
A=196
Q/GeV =
10
7
5
3
2
Q = p_T
R_G^A
$\sqrt{s}$=200 GeV
$\sqrt{s}$=6500 GeV
Ansatz 2
$R_G^A(x, Q)$
x
1.2
1.1
1.0
0.9
0.8
0.7
0.6
0.5
0.4
0.3
0.001
0.01
0.1
1

Fig. 7

LAWRENCE BERKELEY LABORATORY
UNIVERSITY OF CALIFORNIA
TECHNICAL INFORMATION DEPARTMENT
BERKELEY, CALIFORNIA 94720